Sub-Doppler and Doppler spectroscopy of DCN isotopomers in the terahertz region: Ground and first excited bending states (v1v 2v3) = (0 1e,f0)

ARTICLE *in* JOURNAL OF MOLECULAR SPECTROSCOPY · JUNE 2004

Impact Factor: 1.48 · DOI: 10.1016/j.jms.2004.02.021

6 AUTHORS, INCLUDING:

Sandra Brünken
University of Cologne
88 PUBLICATIONS **1,049** CITATIONS
SEE PROFILE

Š. Urban
University of Chemistry and Technology, Pr…
90 PUBLICATIONS **1,495** CITATIONS
SEE PROFILE

Thomas F. Giesen
Universität Kassel
136 PUBLICATIONS **1,528** CITATIONS
SEE PROFILE

Available online at www.sciencedirect.com
SCIENCE DIRECT®
Journal of Molecular Spectroscopy 225 (2004) 152–161
Journal of MOLECULAR SPECTROSCOPY
www.elsevier.com/locate/jms

Sub-Doppler and Doppler spectroscopy of DCN isotopomers in the terahertz region: ground and first excited bending states $(v_1 v_2 v_3) = (0\,1^{e,f}\,0)$☆

S. Brünken,[a,*] U. Fuchs,[a] F. Lewen,[a] Š. Urban,[b,c] T. Giesen,[a] and G. Winnewisser[a]

[a] *I. Physikalisches Institut, Universität zu Köln, D-50937 Köln, Germany*
[b] *Department of Analytical Chemistry, Institute of Chemical Technology, Technická 5, 166 28 Prague 6, Czech Republic*
[c] *The J. Heyrovsky Institute of Academy of Sciences, Dolejskova 3, CZ-18223 Prague 8, Czech Republic*

Received 29 December 2003; in revised form 9 February 2004
Available online 19 March 2004

Abstract

The rotational spectra of the deuterium cyanide isotopic species DCN, $D^{13}CN$, $DC^{15}N$, and $D^{13}C^{15}N$ were recorded in the vibrational ground and first excited bending state ($v_2 = 1$) up to 2 THz. The *R*-branch transitions from $J = 3 \leftarrow 2$ to $J = 13 \leftarrow 12$ were measured with sub-Doppler resolution. These very high resolution (~70 kHz) and precise (±3–10 kHz) saturation dip measurements allowed for resolving the underlying hyperfine structure due to the ^{14}N nucleus in DCN and $D^{13}CN$ for transitions as high as $J = 10 \leftarrow 9$. Additional high *J* *R*-branch ($J = 25 \leftarrow 24$ to $J = 28 \leftarrow 27$) transitions around 2 THz and direct *l*-type ($\Delta J = 0$, $J = 19$ to $J = 25$) transitions from 66 to 118 GHz were recorded in Doppler-limited resolution. For the ground state of $D^{13}C^{15}N$, the $J = 1 \leftarrow 0$ transition was measured for the first time. The transition frequency accuracies for the other deuterated species were significantly improved. These new experimental data, together with the available infrared rovibrational data and previously measured direct *l*-type transitions, were subjected to a global least squares analysis for each isotopomer. This yielded precise sets of molecular constants for the ground and first excited vibrational states, including the nuclear quadrupole and magnetic spin–rotation coupling constants of the ^{14}N nucleus for DCN and $D^{13}CN$. The hyperfine structure due to the D, ^{13}C, and ^{15}N nuclei have not been resolved, but led to a broadening of the observed saturation dips.

Keywords: Molecular spectroscopy; Sub-Doppler spectroscopy; High-resolution spectroscopy; Deuterium cyanide; Microwave spectroscopy; THz spectroscopy; Hyperfine structure

1. Introduction

Hydrogen cyanide has been of great astrophysical interest since its first detection (of HCN and $H^{13}CN$) in the interstellar medium in 1971 [1]. The deuterated species DCN[1] and its hyperfine structure were observed soon afterwards towards the Orion star-forming region [2,3]. In the paper presenting this first astrophysical detection of a deuterated species ever, the authors already discussed the overabundance of the D- to the H-containing isotopomers compared to terrestrial values. Isotopic abundance ratios provide insight into the chemical and physical evolution of the interstellar medium. In the case of deuterium-bearing species this has been theoretically discussed in detail in [4] and been applied to the HCN/DCN ratio by Roberts et al. [5] and Hatchell et al. [6]. Although the doubly and triply substituted HCN species $D^{13}CN$, $DC^{15}N$, and $D^{13}C^{15}N$ have not yet been detected in the interstellar medium, this might be feasible in the future with the aid of new, sensitive millimeter- and submillimeter-wave telescopes (e.g., APEX) and in consideration of the recent

☆ Supplementary data associated with this article can be found in the online version at doi:10.1016/j.jms.2004.02.021.

* Corresponding author. Fax: +49-221-470-5162.
E-mail address: bruenken@ph1.uni-koeln.de (S. Brünken).

[1] Letters not carrying a superscript are corresponding to ^{12}C and ^{14}N, respectively.

0022-2852/$ - see front matter © 2004 Elsevier Inc. All rights reserved.
doi:10.1016/j.jms.2004.02.021

detection of several multi-substituted molecules like ND_3 [7] or $^{13}C^{17}O$ [8].

As was pointed out by Boonman et al. [9], rotational transitions corresponding to energetically high levels of HCN isotopomers are well suited to probe the warmer, inner part of molecular cores in star-forming regions with respect to the determination of molecular abundances and thereby for evolutionary effects. So far, the rotational transitions with the highest J-value measured in the interstellar medium are the $J = 9 \leftarrow 8$ transitions in the vibrational ground [10] and the first excited bending state [9] of the main isotopomer HCN. Very recently, Thorwirth et al. [11] were able to observe direct l-type transitions of HCN connecting energetically high-lying levels (up to $J = 14$) at relative low frequencies (<50 GHz).

The first laboratory microwave spectra of hydrogen cyanide isotopes have been reported as early as 1950 by Simmons et al. [12]. The pure rotational spectra of the linear triatomic HCN isotopes exhibit both widely spaced ($B_{DCN} = 36207.4622$ MHz) R-branch ($\Delta J = 1$) transitions and, in the first excited bending state, so-called direct l-type transitions with $\Delta J = 0$. The l-type transitions have been investigated by several authors [13–18] for all deuterated isotopic species to a varying extent. An overview of the rotational data ($\Delta J = 0$ and 1) up to the year 1977 can be found in a compilation made by Lovas [19].

The ^{14}N-containing species show a significant hyperfine splitting for low J rotational lines, mainly due to the electric nuclear quadrupole moment of the nitrogen nucleus, and to a smaller extent to its magnetic spin–rotation interaction. The most recent publications related to this subject are by Nguyen-van-Thanh and Rossi [20] for DCN and Preusser and Maki [21] for all deuterated isotopomers up to 500 GHz. However, the experimental data as presented by Preusser and Maki lacks high accuracy as it was taken with Doppler-limited resolution, whereas high-precision measurements are only available for DCN for the $J = 2 \leftarrow 1$ and $J = 1 \leftarrow 0$ transition [22] and for few direct l-type transitions [18].

Therefore, we started a project to investigate the rotational spectra of eight isotopic species of hydrogen cyanide with sub-Doppler resolution in the vibrational ground and first excited bending state up to 1 THz with the Cologne Terahertz Spectrometer. Furthermore, to constrain the rotational and centrifugal distortion constants and to extend the frequency region where reliable transition frequency predictions are possible, additional Doppler-limited measurements were undertaken in the frequency region from 1.75 to 2.01 THz using the Cologne sideband spectrometer for terahertz applications (COSSTA). The precise prediction of rest frequencies of rotational transitions at high frequencies is necessary especially with regard to the future satellite mission Herschel and the Stratospheric Observatorium for Infrared Astronomy (SOFIA), both equipped with high-resolution receivers up to 2 THz.

In this paper we report the results for the deuterated species DCN, $D^{13}CN$, $DC^{15}N$, and $D^{13}C^{15}N$. The investigation of the H-containing species is published elsewhere [23–25].

2. Experimental setup

Three different spectrometers of the Cologne laboratory were used to cover the various frequency regions: the Cologne Terahertz Spectrometer, the Cologne Sideband Spectrometer for Terahertz Applications, and the lower frequency AMC spectrometer.

All measurements on the deuterated species were performed with isotopically enriched samples (>50%). The sample pressure ranged between 8×10^{-3} and 0.15 Pa for the sub-Doppler measurements, from 0.1 to 1 Pa for the high-frequency R-branch and around 1 Pa for the direct l-type transitions. For these latter measurements the absorption cell was heated to ~500 K. Since not all readers may be familiar with our technical facilities, we offer here a very short overlook of the instrumentation used to cover the frequency region from about 50 GHz to 2 THz.

2.1. The Cologne terahertz spectrometer

In Cologne backward wave oscillators (BWO) from the ISTOK company in Russia with high output power (1–100 mW) are used to generate millimeter- and submillimeter-radiation of high-spectral purity. A frequency stability in the sub-kHz domain is realised by down-converting and phase-locking a fraction of the BWO radiation to an atomic clock reference signal, thereby allowing for the very accurate determination of molecular transition frequencies in a broad frequency range from 180 to 1200 GHz. A detailed description of the experimental setup is given in [26,27]. The achieved frequency accuracy of a measured rotational transition is mainly affected by various factors caused by the mode of observation ($2f$-modulation of the source frequency), baseline effects due to standing waves and the strength of the observed line and ranges from 10 to 100 kHz in Doppler- and from 3 to 20 kHz in sub-Doppler mode.

2.2. Saturation dip measurements and accompanying crossover dips

In the case of two electromagnetic waves travelling in opposite directions through an absorbing gas (i.e., pump and probe beam), the absorption pattern corresponding to the spectrum recorded with the probe beam can

exhibit a narrow dip at the centre frequency of the transition due to power saturation. The linewidth of these so-called Lamb dips [28] is in the ideal case close to the transitions natural linewidth.

To perform saturation dip measurements with the Cologne Terahertz Spectrometer we performed a little trick: a part of the incoming BWO radiation is reflected at the surface of the detector element (InSb hot electron bolometer) and with a careful optical adjustment guided back through the absorption cell. This reflected radiation acts as the pump beam, whereas the initial incoming wave is the probe beam. The relative intensity of the generated dip is proportional to $(\mu_{12}E)^4$, where E is the intensity of the monochromatic electromagnetic field and μ_{12} is the transition dipole matrix moment of the observed line.

The high power radiation provided by the BWO sources is required for obtaining saturation dip conditions for very low DCN sample pressures even in the case of intense rotational transitions.

Both the sample pressure and the radiation power have carefully been adjusted for each measurement to avoid pressure (collisional) and power broadening effects. Furthermore, the amplitude of the frequency modulation was chosen very low to avert influences on the linewidth. Further information about the Cologne sub-Doppler measurements can be found in [29,30].

2.3. COSSTA

Sideband radiation is generated by mixing the output radiation of a phase-stabilised BWO with frequency-stabilised radiation of a FIR ring-laser system operated at a fixed frequency of 1.626 THz. Since the BWOs used can be continuously tuned within a frequency range from ~130 to 390 GHz, the produced sideband radiation (at a frequency given by the sum of BWO and FIR-laser frequency) covers a frequency region from 1.75 to 2.01 THz. The frequency stability is limited by the loop error of the automatic frequency control (AFC) stabilising the FIR laser and was determined to be <5 kHz. A more detailed description is given in [31,32].

2.4. AMC spectrometer

In the low frequency region (54–180 GHz) the commercial, BWO-based AMC spectrometer (Analytik und Messtechnik GmbH, Chemnitz) was utilised to measure the $J = 1 \leftarrow 0$ rotational transition and several direct l-type transitions. The AMC spectrometer can be operated with different BWO tubes in the range from 54 to 178 GHz. Due to the significantly lower output power of a few mW and an intrinsic linewidth of a few kHz it was not possible to perform saturation dip measurements using this spectrometer.

3. Measurements

About 40 rotational transitions have been measured for each of the four hydrogen cyanide isotopomers DCN, $D^{13}CN$, $DC^{15}N$, and $D^{13}C^{15}N$ in the vibrational ground and first excited bending state making use of the three spectrometers described in the previous section. The recorded spectra vary according to molecular and spectrometer characteristics. Figs. 1–10 display exemplary spectra for each frequency region. As it will be elucidated in more detail in the next section, for the isotopic species containing the ^{14}N ($I_N = 1$) nucleus each

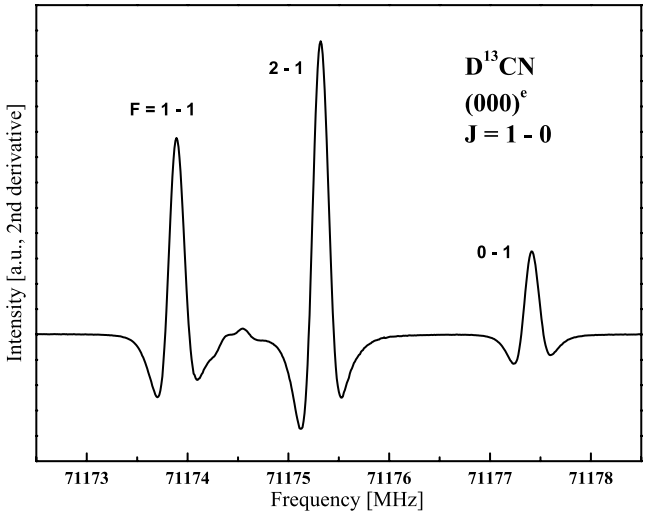

Fig. 1. The $J = 1 \leftarrow 0$ rotational transition of $D^{13}CN$ in the ground vibrational state recorded with Doppler-limited resolution employing the AMC spectrometer. The three allowed hyperfine components are labelled.

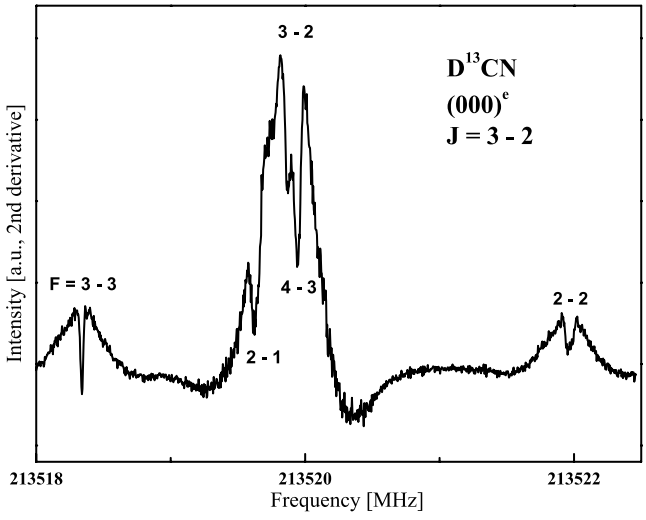

Fig. 2. The $J = 3 \leftarrow 2$ rotational transition of $D^{13}CN$ in the vibrational ground state recorded with sub-Doppler resolution with the Cologne Terahertz spectrometer. The five strongest saturation dips are resolved and identified.

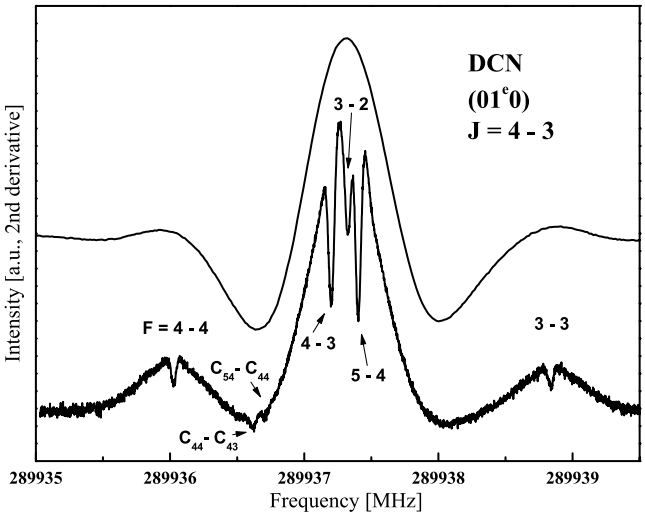

Fig. 3. The $J = 4 \leftarrow 3$ rotational transition of DCN in the first excited bending state ($0\,1^e\,0$) recorded with sub-Doppler resolution. For comparison, a Doppler-limited recording of the same transition is presented.

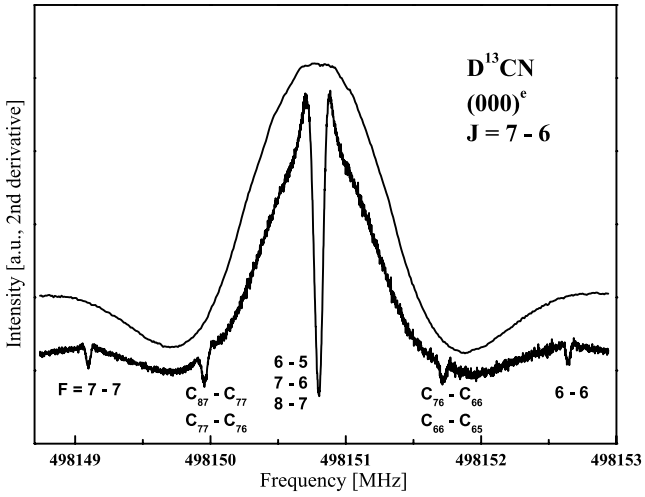

Fig. 4. The $J = 7 \leftarrow 6$ rotational transition of $D^{13}CN$ in the vibrational ground state recorded with sub-Doppler resolution. The inner hyperfine components can no longer be resolved. Two visible crossover dips (explanation see text) are labelled.

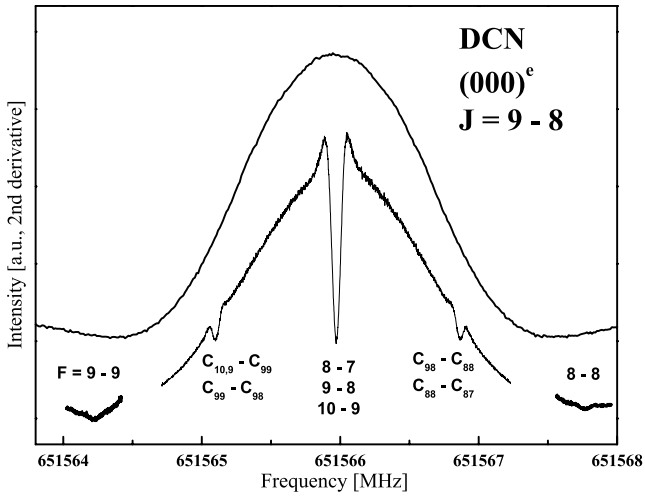

Fig. 5. The $J = 9 \leftarrow 8$ rotational transition of DCN in the vibrational ground state recorded in sub-Doppler resolution. The intensity of the $\Delta F = 0$ components decreases faster than those of the $\Delta F = 1$ transitions.

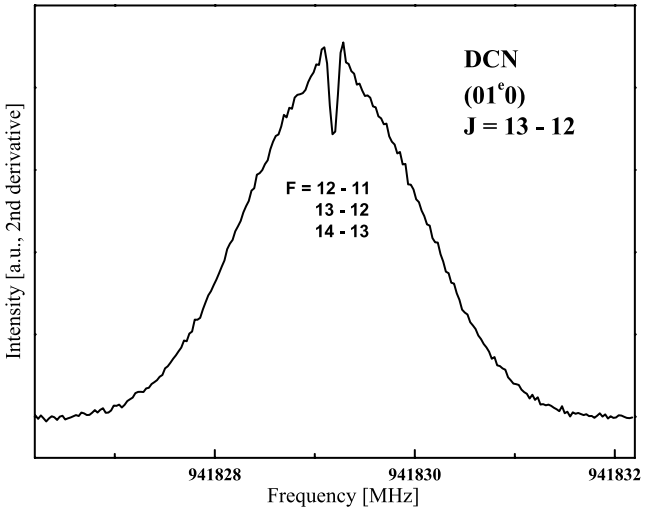

Fig. 6. The $J = 13 \leftarrow 12$ rotational transition of DCN in the $v_2 = 1^e$ state is one of the highest transitions measured in sub-Doppler resolution. Only the unresolved inner hyperfine triplet can be seen superimposed on the Doppler broadened lineshape.

rotational energy level (with the exception of the $J = 0$ state) is split into a triplet. This splitting causes a noticeable hyperfine structure in the low frequency rotational spectra. The lowest $J = 1 \leftarrow 0$ ground state transition, a hyperfine triplet, can be fully resolved with Doppler-limited techniques as shown in Fig. 1. According to the electric dipole selection rules ($\Delta F = 0, \pm 1$) the theoretical hyperfine pattern of all higher J transitions consists of a hyperfine sextet. Since the $\Delta F = -1$ transitions were too weak to be resolved in this experiment, Figs. 2 and 3 show only five saturation dips. The three $\Delta F = +1$ hyperfine components form a closely confined inner triplet, whereas the two $\Delta F = 0$ transitions are clearly separated and more widely spaced. In Fig. 3 a recorded Doppler-limited spectrum is superimposed on the corresponding saturation dip records, showing no trace of the underlying hyperfine structure.

In the sequence of Figs. 3–6 three characteristics of the performed saturation dip measurements are exemplified:

(i) With increasing J-value the separation of the inner $\Delta F = 1$ components decreases.[2] In the case of the

[2] This behaviour is determined by the nuclear hyperfine constants (see Section 4), therefore it differs in the ground and first excited bending state. The order of the hyperfine components is different in both states and for the $v_2 = 1^{e,f}$ the aforementioned assertion is not strictly true in the case of small J.

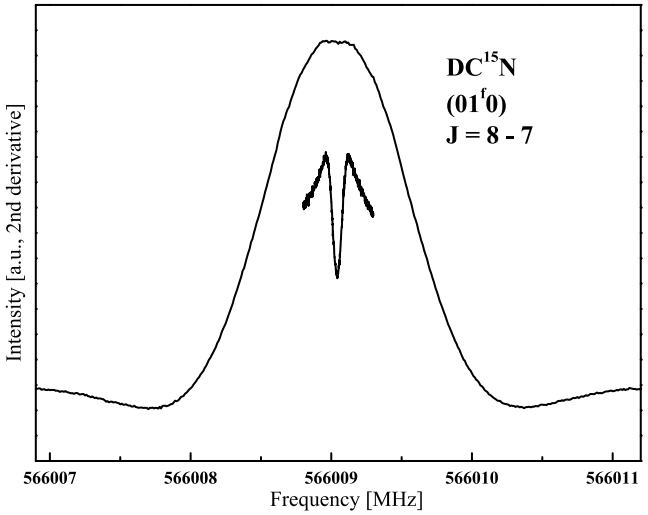

Fig. 7. The $J = 8 \leftarrow 7$ rotational transition of $DC^{15}N$ in the $v_2 = 1^f$ state recorded in Doppler and sub-Doppler resolution is shown for comparison.

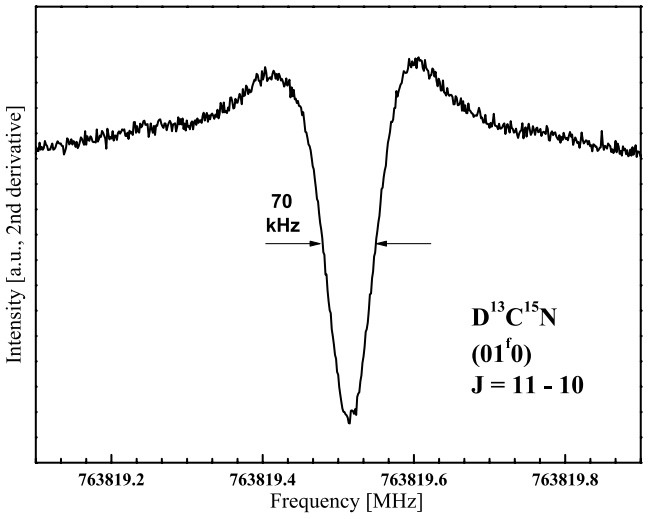

Fig. 8. The $J = 11 \leftarrow 10$ rotational transition of the rare isotopomer $D^{13}C^{15}N$ in the $v_2 = 1^f$ state recorded in sub-Doppler resolution. The linewidth (FWHM) of the second derivative of the saturation dip is ~70 kHz.

displayed $D^{13}CN$ $J = 7 \leftarrow 6$ transition (Fig. 4) the separation of the hyperfine components is only ~20 kHz and thereby below the achieved sub-Doppler resolution of ~50 kHz.

(ii) The intensity of the observed $\Delta F = 0$ hyperfine transitions decrease faster with J than the corresponding $\Delta F = 1$ transitions (relative intensity $\sim 1/J^2$) and could therefore be detected only up to $J = 9 \leftarrow 8$.

(iii) For intermediate values of J (Figs. 3–5) additional saturation dips appear in the spectra. These so-called crossover dips are generated if the incoming and the reflected wave interact with the same velocity class of molecules but via different transitions sharing one common level. Since this can only happen if the frequency separation of the two participating transitions is smaller than the Doppler linewidth (and the Doppler linewidth increases with frequency), no crossover dips appear in Fig. 2, because in this case the separation of the corresponding hyperfine components is too large. The labelling of the dips is done according to the participating hyperfine transitions, e.g., the $C_{87} - C_{77}$ saturation dip is generated by the $J_F : 7_8 \leftarrow 6_7$ and $7_7 \leftarrow 6_7$ transitions, thereby sharing a common lower level. The crossover dips occur at the arithmetic average frequency of the involved hyperfine components and might therefore be helpful to obtain additional frequency information, since only one of the unresolved $\Delta F = 1$ triplet components forms a crossover dip with a $\Delta F = 0$ transition. There is, however, in general an overlap of two crossover dips (one connecting states of common lower, one of common upper level).[3] A more detailed analysis of the theory of crossover dips can be found in [23].

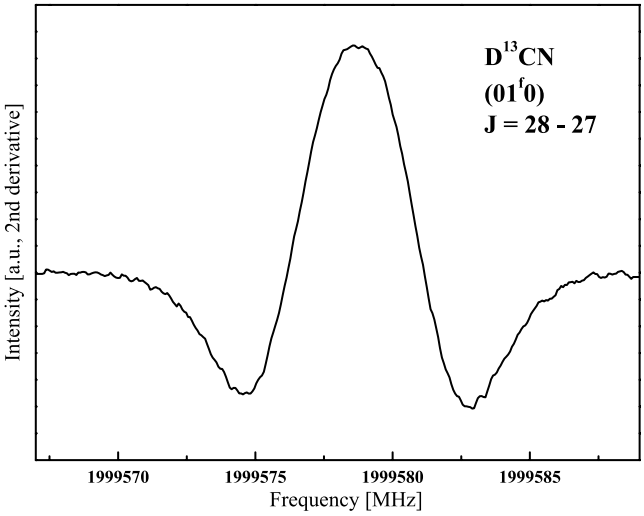

Fig. 9. Exemplary spectrum recorded with COSSTA around 2 THz of the $J = 28 \leftarrow 27$ rotational transition of $D^{13}CN$ in the $v_2 = 1^f$ vibrational state.

Although the two isotopic species $DC^{15}N$ and $D^{13}C^{15}N$ do not exhibit a measurable hyperfine structure, they were nevertheless measured in sub-Doppler resolution in the frequency range from 400 to 900 GHz with the objective of improved frequency accuracy (a factor of 5–10 for most lines). Exemplary spectra are shown in Figs. 7 and 8.

[3] It is to be noted that the frequency difference of the two generated crossover dips is half that of the involved $\Delta F = 1$ components. Lines that are resolved in the saturation dips therefore might not be resolved in the crossover dips.

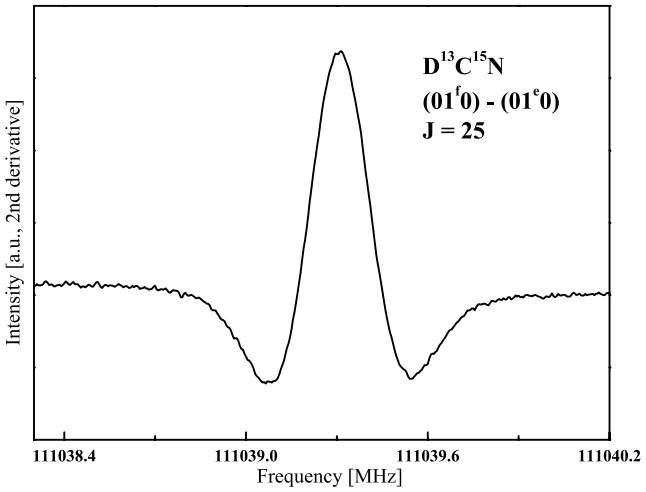

Fig. 10. Exemplary spectrum of a direct l-type transition ($\Delta J = 0$, $t_J = 25$) of $D^{13}C^{15}N$ with $E_{up} = 1312.35\,cm^{-1}$. According to the selection rules, this transition connects the $(0\,1^e\,0)$ and $(0\,1^f\,0)$ vibrational states.

Both the transitions in the high-frequency region (1.75–2.01 THz, Fig. 9) and the direct l-type transitions (Fig. 10) were recorded in Doppler resolution.

The splittings due to the D, ^{13}C, and ^{15}N nuclear spin–rotation, electric quadrupole coupling and spin–spin interactions were not resolved in our experiments. We performed, however, calculations including the interaction of all participating nuclei. The corresponding constants have been calculated from nuclear spin–rotation and nuclear electric quadrupole coupling constants of DCN, $DC^{15}N$ and $D^{13}CN$ published by DeLucia and Gordy [22], Cazzoli and Dore [33], and Garvey and De Lucia [34], respectively. Whereas the found splitting of the strong hyperfine components lies with a few kHz well below the achieved sub-Doppler resolution, it might cause a substantial broadening of the lines.

A short summary of the dataset obtained in this study is given in Table 1, indicating especially which measurements were performed with sub-Doppler resolution. Tables containing all experimental transition frequencies used in the analysis can be found in the electronic supplement to this article (Tables 7–15). An excerpt is shown in Table 2 for the first excited bending state of DCN.

Table 1
Summary of the measurements performed with the different Cologne spectrometers on DCN isotopomers in the vibrational ground (0 0 0) and first excited state (0 1 0)

	Low frequency[a] 66–117 GHz (AMC)	Sub-Doppler 207–960 GHz (THz-spectrometer)	High frequency 1.75–2.01 THz (sideband-spectrometer)
DCN	$J = 19, 20, 22$–24	$(0\,0\,0)$ $J'' = 2$–12	$(0\,0\,0)$, $(0\,1\,0)$ $J'' = 25, 26$
	$J'' = 0$	$(0\,1\,0)$ $J'' = 2$–$3, 5$–$9, 11$–12	
$D^{13}CN$	$J = 19$–25	$(0\,0\,0)$ $J'' = 2$–12	$(0\,0\,0)$, $(0\,1\,0)$ $J'' = 26, 27$
	$J'' = 0$	$(0\,1\,0)$ $J'' = 2$–12	
$DC^{15}N$	$J = 19$–25	$(0\,0\,0)$ $J'' = 2$–$6, 8$–12	$(0\,0\,0)$, $(0\,1\,0)$ $J'' = 24$–27
	$J'' = 0$	$(0\,1\,0)$ $J'' = 2$–$9, 11$–12	
$D^{13}C^{15}N$	$J = 19$–25	$(0\,0\,0)$ $J'' = 2$–$6, 8$–12	$(0\,0\,0)$, $(0\,1\,0)$ $J'' = 25$–28
	$J'' = 0$	$(0\,1\,0)$ $J'' = 2$–$6, 8$–12	

J'' denotes the lower energy level of the rotational transitions.
[a] In the first row, direct l-type transitions are summarised ($\Delta J = 0$).

Table 2
Excerpt from the list of experimentally derived transition frequencies of DCN

J'	F'	J''	F''	ν_{exp} (MHz) (σ)	o − c (MHz)	$I_{abs,lin}$	$I_{rel,lin}$	$I_{abs,sat}$	$I_{rel,sat}$
				...					
8	←	7	(*e*)	579784.4432(0025)					
8	8/9	7	8/8	579783.628(010)	−0.005			3.1E+03	0.01
8	8/8	7	8/7	579783.628(010)	−0.005			3.1E+03	0.01
8	7	7	6	579784.448(005)	0.020	1.7E+03	14.44	3.0E+06	12.61
8	8	7	7	579784.448(005)	0.020	2.0E+03	16.41	3.9E+06	16.27
8	9	7	8	579784.448(005)	−0.021	2.2E+03	18.63	5.0E+06	20.98
8	8/7	7	7/7	579785.295(010)	0.010			2.0E+03	0.01
8	7/7	7	7/6	579785.295(010)	0.010			1.7E+03	0.01
				...					

For each transition a calculated hyperfine free rotational frequency is given (standard deviation (σ) is given in parentheses); e or f denote the vibrational state $(0\,1^{e,f}\,0)$. Calculated intensities both for the linear and saturation experiment in relative and absolute values are given for each hyperfine transition. The absolute values are the dimensionless intrinsic line strengths. It is to be noted that crossover dips do not exist in linear spectroscopy.

4. Analysis

The experimentally obtained transition frequencies were subjected to a least squares analysis using the program code developed by Pickett et al. [35]. The utilised expansion terms of the energy expression will be described in detail in the following sections.

The derived spectroscopic constants are collected in Tables 3–6 and compared to previous published values by Preusser and Maki [21] and Quapp et al. [36], respectively, Möllmann et al. [37]. As a supplement to the newly measured transition frequencies, most of the to date published data on rotational transitions of the deuterium cyanide isotopomers have been included in our fit. These additional data consist in detail of the $J = 2 \leftarrow 1$ rotational transition frequencies measured by DeLucia and Gordy [22], Winnewisser et al. [38] (DCN), Pearson et al. [39] ($D^{13}CN$), and Preusser and Maki [21] ($D^{13}CN$, $DC^{15}N$, and $D^{13}C^{15}N$) and direct *l*-type transitions given in Fliege et al. [18], Maki and Lide [16] (DCN, $DC^{15}N$) and Törring [15] (DCN, $D^{13}CN$, and $DC^{15}N$). Furthermore, the infrared $(0\,1^{e,f}\,0) \leftarrow (0\,0\,0)$

Table 3
High precision rotational and hyperfine constants of DCN in the vibrational ground and first excited bending state

Parameter	This work	Möllmann et al. [37]	Preusser and Maki [21]
$v_2 = 0$			
B_0 (MHz)	36207.462159(126)	36207.46259(24)	36207.46226(20)
D_0 (kHz)	57.74140(73)	57.7652(27)	57.730(14)
H_0 (Hz)	0.07326(63)	0.0831(11)	
eQq_0 (MHz)	−4.6934(49)		−4.698(7)
$eQq_{J,0}$ (kHz)	0.349(115)		
$C_{N,0}$ (kHz)	8.63(31)		[8.23]
$v_2 = 1$			
B_1 (MHz)	36337.020129(111)	36337.02330(60)	36337.0231(13)
D_1 (kHz)	59.83231(65)	59.8587(28)	59.852(24)
H_1 (Hz)	0.09682(59)	0.1071(11)	
eQq_1 (MHz)	−4.7972(76)		−4.796(8)
$eQq_{J,1}$ (kHz)	0.349(115)		
$eQq\eta$ (kHz)	346.1(80)		[339]
$C_{N,1}$ (kHz)	8.82(35)		[8.23]
q (MHz)	186.190702(51)	186.190822(12)	186.1908901(115)
q_J (kHz)	2.201498(192)	2.20176(12)	2.20278(15)
q_{JJ} (Hz)	0.041978(156)	0.04269(14)	0.04378(17)
E (MHz)	17095750.65(32)	17095750.50(54)	
wrms	0.955		

Values in square brackets were fixed.

Table 4
High precision rotational and hyperfine constants of $D^{13}CN$ in the vibrational ground and first excited bending state

Parameter	This work	Möllmann et al. [37]	Preusser and Maki [21]
$v_2 = 0$			
B_0 (MHz)	35587.645800(182)	35587.6508(18)	35587.6479(19)
D_0 (kHz)	55.57890(96)	55.617(14)	55.576(35)
H_0 (Hz)	0.06300(80)	0.0770(72)	
eQq_0 (MHz)	−4.6972(49)		−4.703(16)
$eQq_{J,0}$ (kHz)	0.224(102)		
$C_{N,0}$ (kHz)	7.01(34)		[8.23]
$v_2 = 1$			
B_1 (MHz)	35707.049846(161)	35707.0554(14)	35707.0571(13)
D_1 (kHz)	57.46879(83)	57.507(13)	57.529(25)
H_1 (Hz)	0.08348(76)	0.0968(69)	
eQq_1 (MHz)	−4.7848(47)		−4.795(20)
$eQq_{J,1}$ (kHz)	0.224(102)		
$eQq\eta$ (kHz)	334.4(50)		[339]
$C_{N,1}$ (kHz)	6.77(30)		[8.23]
q (MHz)	182.294230(124)	182.29421(27)	182.29427(32)
q_J (kHz)	2.07675(31)	2.07696(81)	2.0775(20)
q_{JJ} (Hz)	0.037304(202)	0.03783(69)	0.0386(25)
E (MHz)	16864069.24(34)	16864069.34(63)	
wrms	1.09		

Values in square brackets were fixed.

Table 5
High precision rotational and hyperfine constants of $DC^{15}N$ in the vibrational ground and first excited bending state

Parameter	This work	Preusser and Maki [21]
$v_2 = 0$		
B_0 (MHz)	35169.797904(261)	35169.79976(6)
D_0 (kHz)	54.39237(151)	54.392(17)
H_0 (Hz)	0.06330(123)	
wrms	0.45192	
$v_2 = 1$		
B_1 (MHz)	35294.750863(193)	35294.7545(16)
D_1 (kHz)	56.33892(115)	56.354(30)
H_1 (Hz)	0.08815(100)	
q (MHz)	176.080934(88)	176.081035(62)
q_J (kHz)	2.01282(35)	2.01329(115)
q_{JJ} (Hz)	0.03867(36)	0.0366(45)
wrms	0.744	

data by Möllmann et al. [37] (DCN, $D^{13}CN$) and Quapp et al. [36] ($D^{13}C^{15}N$) have been included.

In those cases where additional splitting of the rotational lines due to the D, ^{13}C, and ^{15}N nuclei was observed [22,33,34], either intensity weighted mean frequencies or data from in parallel existing studies not resolving the splitting were used in the fit (see Tables 7–16 of the electronic supplementary material).

4.1. Ground state

For calculating the rotational energy eigenvalues of a linear molecule in the vibrational ground state, taking only the interaction of the ^{14}N nucleus into account, the following approximation has been used:

$$\begin{aligned}\frac{E}{h} &= \frac{E_{\mathrm{rot}}}{h} + \frac{E_{\mathrm{HFS}}}{h} \\ &= B_0 J(J+1) - D_0 J^2(J+1)^2 + H_0 J^3(J+1)^3 \\ &\quad + eQq_0 \cdot Y(J,I,F) + eQq_{J,0} J(J+1) \cdot Y(J,I,F) \\ &\quad + \frac{C_{I,0}}{2} \cdot C. \end{aligned} \tag{1}$$

Here B, D, and H, denote the rotational spectroscopic constants, eQq is the nuclear electric quadrupole coupling constant, eQq_J its first centrifugal correction, C_I the magnetic spin–rotation coupling constant, $\vec{F} = \vec{J} + \vec{I}$ the total angular momentum,

$$Y(J,I,F) = \frac{\frac{3}{4}C(C+1) - I(I+1)J(J+1)}{2(2J-1)(2J+3)I(2I-1)},$$

and $C = F(F+1) - J(J+1) - I(I+1)$ Casimir's function. For $DC^{15}N$ and $D^{13}C^{15}N$ only the first three terms of Eq. (1) are to be considered, because of the missing nitrogen quadrupole moment and the negligible magnetic spin–rotation coupling.

All the coupling constants as well as the spin quantum number $\vec{I}$ are assigned to the nitrogen nucleus. Effects of the deuterium quadrupole moment and magnetic spin have been ignored, as well as any interactions resulting from the ^{13}C or ^{15}N nuclear magnetic spin.

4.2. First excited bending state

In the excited bending states the interaction of the vibration with the rotation has to be taken into account. This leads to a splitting of each rotational line. The energy expression has to be adjusted and now reads for the first excited bending state:

$$\begin{aligned}\frac{E^{\pm}}{h} &= \frac{E_{\mathrm{vib}}}{h} + \frac{E_{1,\mathrm{rot}}}{h} + \frac{E_{1,\mathrm{HFS}}}{h} \\ &= G_0 + B_1[J(J+1) - l^2] - D_1[J(J+1) - l^2]^2 \\ &\quad + H_1[J(J+1) - l^2]^3 \pm \frac{q}{2} J(J+1) \\ &\quad \mp \frac{q_J}{2} J^2(J+1)^2 \pm \frac{q_{JJ}}{2} J^3(J+1)^3 \\ &\quad + eQq_1 Y(J,I,F)\left[\frac{3l^2}{J(J+1)} - 1 \pm \frac{\eta}{2}\right] \\ &\quad - eQq_{J,1} J(J+1) Y(J,I,F)\left[\frac{3l^2}{J(J+1)} - 1\right] + \frac{C_{I,1}}{2} C, \end{aligned} \tag{2}$$

Table 6
High precision rotational and hyperfine constants of $D^{13}C^{15}N$ in the vibrational ground and first excited bending state

Parameter	This work	Quapp et al. [36]	Preusser et al. [21]
$v_2 = 0$			
B_0 (MHz)	34531.299725(184)	34531.3005(19)	34531.3019(9)
D_0 (kHz)	52.26535(96)	52.245(11)	52.279(14)
H_0 (Hz)	0.06074(73)	0.0564(45)	
$v_2 = 1$			
B_1 (MHz)	34646.234158(177)	34646.2356(15)	34646.2382(7)
D_1 (kHz)	54.01254(95)	53.991(11)	54.033(13)
H_1 (Hz)	0.07816(75)	0.0734(42)	
q (MHz)	172.044884(124)	172.04503(25)	172.045118(135)
q_J (kHz)	1.89128(45)	1.89124(66)	1.89173(79)
q_{JJ} (Hz)	0.03349(42)	0.03313(48)	0.0336(9)
E (MHz)	16825097.29(74)	16825101.2(14)	
wrms	0.992		

with $l^2 = 1$ in the first excited bending vibrational state. Additional fitting parameters are the l-type doubling constant q, its centrifugal distortion corrections q_J and q_{JJ}, and the asymmetry parameter η. The value of the last parameter can be deduced from the parameter $eQq\eta = eQq \times \eta$ in Tables 3–6. It should be noted that the influence of the vibrational angular momentum on the magnetic coupling constant C_l has been omitted in the fit, the difference being too small to be determinable. Furthermore, from the infrared data [36,37], the constant $G_0 = G(v, l) - G(0, 0)$ could be derived. The subscripts 0 and 1 denote the ground and first excited bending state, respectively.

According to the scheme proposed by Brown et al. [40], the rotational levels are labelled according to their energy ordering by e and f, i.e., there exist two vibrational states ($0\,1^{e,f}\,0$), the rotational energy levels in the ($0\,1^{e}\,0$) state corresponding to E^-, those in the ($0\,1^{f}\,0$) state to E^+.[4]

5. Discussion

The combination of the newly measured transitions with existing data yields the most comprehensive dataset on the deuterium cyanide isotopomers DCN, D^{13}CN, DC^{15}N, and D^{13}C^{15}N to date. The accuracy of the rotational spectroscopic and centrifugal distortion constants B, D, and H could be improved compared to previously published values [21,36,37] by a factor of 10 for all isotopomers for both the vibrational ground and first excited state. The improvement in the accuracy of the l-type doubling constants is only a factor of two compared to that stated by Quapp et al. [36] and Möllmann et al. [37] deduced from infrared emission data alone. This is not surprising, since their data include transitions involving rotational quantum numbers up to $J = 62$.

For the two ^{14}N-containing species the first centrifugal correction to the electric quadrupole coupling constants $eQq_{J,0}$ ($eQq_{J,1}$ was fixed to the same value during the fit), the asymmetry parameter of the electric field gradient η (i.e., $eQq\eta$) and the magnetic coupling constants $C_{N,0}$ and $C_{N,1}$ have been determined for the first time. The accuracy of the electric quadrupole coupling constants $eQq_{0,1}$ could be improved by a factor of 4–10.

The newly calculated, highly accurate parameter set was employed to predict rotational transitions in the ground and first excited bending state of all four isotopomers. The predicted frequency uncertainty for fairly strong transitions is less than 100 kHz for frequencies up to 2.5 THz and generally less than 30 kHz in the intermediate frequency region not covered by the present high-resolution measurements. The full calculated transition frequencies, including hyperfine splitting, will be published in the internet in the Cologne Database for Molecular Spectroscopy (CDMS) at www.cdms.de. These line predictions may prove helpful in the analysis of future far infrared high frequency and spatial resolution astronomical observations, e.g., with SOFIA and Herschel.

[4] The sign of the l-type doubling constants q and $eQq\eta$ depends upon the arbitrary choice of the phases of the wavefunctions [41]. In our case and with the ± designation as given in Eq. (2), both q and $eQq\eta$ are positive. Since eQq_1 is negative, this results in the observed bigger hyperfine splitting in the $v_2 = 1^e$ compared to that in the $v_2 = 1^f$ state.

Acknowledgments

The authors thank J. Suhr and Professor J. Hahn of the Institut für Anorganische Chemie of the Universität zu Köln for the synthesis of the hydrogen cyanide species. We are indebted to H.S.P. Müller for the advice regarding the fitting procedure. The Cologne group has been supported by the Deutsche Forschungsgemeinschaft via research Grants SFB-494. We much acknowledge the Ministry of Science of the Land Nordrhein-Westfalen/Germany for additional financial support. Š.U. acknowledges support through the Grant Agency of the Czech Republic (#203/01/1274). The collaborative work between the Cologne and Prague groups has been additionally supported by the International Office of the Federal Ministry of Education and Science at the DLR via Grant CZE 00/030.

References

[1] L.E. Snyder, D. Buhl, ApJL 163 (1971) L47.
[2] K.B. Jefferts, A.A. Penzias, R.W. Wilson, ApJL 179 (1973) L57.
[3] R.W. Wilson, A.A. Penzias, K.B. Jefferts, P.M. Solomon, ApJL 179 (1973) L107.
[4] S.D. Rodgers, T.J. Millar, MNRAS 280 (1996) 1046–1054.
[5] H. Roberts, G.A. Fuller, T.J. Millar, J. Hatchell, J.V. Buckle, Astron. Astrophys. 381 (2002) 1026–1038.
[6] J. Hatchell, T.J. Millar, S.D. Rodgers, Astron. Astrophys. 332 (1998) 695–702.
[7] D.C. Lis, E. Roueff, M. Gerin, T.G. Phillips, L.H. Coudert, F.F.S. van der Tak, P. Schilke, ApJL 571 (2002) L55–L58.
[8] F. Bensch, I. Pak, J.G.A. Wouterloot, G. Klapper, G. Winnewisser, ApJL 562 (2001) L185–L188.
[9] A.M.S. Boonman, R. Stark, F.F.S. van der Tak, E.F. van Dishoeck, P.B. van der Wal, F. Schäfer, G. de Lange, W.M. Laauwen, ApJL 553 (2001) L63–L67.
[10] J. Stutzki, R. Genzel, A.I. Harris, J. Herman, D.T. Jaffe, ApJL 330 (1988) L125–L129.
[11] S. Thorwirth, F. Wyrowski, P. Schilke, K.M. Menten, S. Brünken, H.S.P. Müller, G. Winnewisser, ApJL 586 (2003) 338–343.
[12] J.W. Simmons, W.E. Anderson, G. Gordy, Phys. Rev. 77 (1950) 77–79.
[13] A. Miyahara, H. Hirakawa, K. Shimoda, J. Phys. Soc. Japan 11 (1956) 335.

[14] H. Hirakawa, T. Oka, K. Shimoda, J. Phys. Soc. Japan 11 (1956) 1208.
[15] T. Törring, Z. Phys. 161 (1961) 179.
[16] A.G. Maki, D.R. Lide, J. Chem. Phys. 47 (1967) 3206.
[17] M. Winnewisser, J. Vogt, Z. Naturforsch. A 33 (1978) 1323–1327.
[18] E. Fliege, H. Dreizler, A.P. Cox, S.D. Hubbard, Z. Naturforsch. A 39 (1984) 1104–1107.
[19] F.J. Lovas, J. Phys. Chem. Ref. Data 7 (1978) 1445–1750.
[20] Nguyen-van-Thanh, I. Rossi, J. Mol. Spectrosc. 157 (1993) 68–83.
[21] J. Preusser, A.G. Maki, J. Mol. Spectrosc. 162 (1993) 484–497.
[22] F. DeLucia, W. Gordy, Phys. Rev. 187 (1969) 58–65.
[23] V. Ahrens, F. Lewen, S. Takano, G. Winnewisser, V. Urban, A.A. Negirev, A.N. Koroliev, Z. Naturforsch. A 57 (2002) 669–681.
[24] S. Thorwirth, H.S.P. Müller, F. Lewen, S. Brünken, V. Ahrens, G. Winnewisser, ApJL 585 (2003) L161–L165.
[25] U. Fuchs, S. Brünken, F. Lewen, S. Thorwirth, G. Winnewisser, J. Mol. Spectrosc., submitted.
[26] G. Winnewisser, A.F. Krupnov, M.Y. Tretyakov, M. Liedtke, F. Lewen, A.H. Saleck, R. Schieder, A.P. Shkaev, S.V. Volokhov, J. Mol. Spectrosc. 165 (1994) 489–494.
[27] G. Winnewisser, Vib. Spectrosc. 8 (1995) 241–253.
[28] W.E. Lamb, Phys. Rev. 134 (1964) 1429.
[29] H. Klein, F. Lewen, R. Schieder, J. Stutzki, G. Winnewisser, ApJL 494 (1998) L125.
[30] G. Klapper, F. Lewen, R. Gendriesch, S.P. Belov, G. Winnewisser, J. Mol. Spectrosc. 201 (2000) 124–127.
[31] F. Lewen, E. Michael, J. Stutzki, G. Winnewisser, J. Mol. Spectrosc. 183 (1997) 207.
[32] R. Gendriesch, F. Lewen, G. Winnewisser, J. Hahn, J. Mol. Spectrosc. 203 (2000) 205–207.
[33] G. Cazzoli, L. Dore, J. Mol. Spectrosc. 143 (1990) 231–236.
[34] R.M. Garvey, F.D. De Lucia, J. Mol. Spectrosc. 50 (1974) 38–44.
[35] H.M. Pickett, R.L. Poynter, E.A. Cohen, M.L. Delitsky, J.C. Pearson, H.S.M. Müller, J. Quant, Spectrosc. Radiat. Transfer 60 (5) (1998) 883–890.
[36] W. Quapp, M. Hirsch, G.C. Mellau, S. Klee, M. Winnewisser, A. Maki, J. Mol. Spectrosc. 195 (1999) 284–298.
[37] E. Möllmann, A.G. Maki, M. Winnewisser, B.P. Winnewisser, W. Quapp, J. Mol. Spectrosc. 212 (2002) 22–31.
[38] M. Winnewisser, A.G. Maki, D.R. Johnson, J. Mol. Spectrosc. 39 (1971) 149.
[39] E.F. Pearson, R.A. Creswell, M. Winnewisser, G. Winnewisser, Z. Naturforsch. A 31 (1976) 1394–1397.
[40] J.M. Brown, J.T. Hougen, K.P. Huber, J.W.C. Johns, I. Kop, H. Lefebvre-Brion, A.J. Merer, D.A. Ramsey, J. Rostas, R.N. Zare, J. Mol. Spectrosc. 55 (1975) 500.
[41] K. Yamada, Z. Naturforsch. A 38 (1983) 821–834.